ANNUAL REVIEWS

Annual Review of Earth and Planetary Sciences

Fracture, Friction, and Permeability of Ice

Erland M. Schulson[1] and Carl E. Renshaw[2]

[1]Thayer School of Engineering, Dartmouth College, Hanover, New Hampshire, USA; email: erland.m.schulson@dartmouth.edu

[2]Department of Earth Sciences, Dartmouth College, Hanover, New Hampshire, USA

Annu. Rev. Earth Planet. Sci. 2022. 50:323–43

The *Annual Review of Earth and Planetary Sciences* is online at earth.annualreviews.org

https://doi.org/10.1146/annurev-earth-032320-085507

Keywords

ice, brittle failure, friction, permeability

Abstract

Water ice Ih exhibits brittle behavior when rapidly loaded. Under tension, it fails via crack nucleation and propagation. Compressive failure is more complicated. Under low confinement, cracks slide and interact to form a frictional (Coulombic) fault. Under high confinement, frictional sliding is suppressed and adiabatic heating through crystallographic slip leads to the formation of a plastic fault. The coefficient of static friction increases with time under load, owing to creep of asperities in contact. The coefficient of kinetic (dynamic) friction, set by the ratio of asperity shear strength to hardness, increases with velocity at lower speeds and decreases at higher speeds as contacts melt through frictional heating. Microcracks, upon reaching a critical number density (which near the ductile-to-brittle transition is nearly constant above a certain strain rate), form a pathway for percolation. Additional work is needed on the effects of porosity and crack healing.

- An understanding of brittle failure is essential to better predict the integrity of the Arctic and Antarctic sea ice covers and the tectonic evolution of the icy crusts of Enceladus, Europa, and other extraterrestrial satellites.
- Fundamental to the brittle failure of ice is the initiation and propagation of microcracks, frictional sliding across crack faces, and localization of strain through both crack interaction and adiabatic heating.

1. INTRODUCTION

The purpose of this review is to examine progress in both characterizing and understanding the brittle failure of ice, with a view to charting the path forward. Friction plays a fundamental role in compressive failure and so is included, as is permeability, as microcracking is an effective means of creating interconnecting pathways.

Unless otherwise noted, most of the results discussed were obtained in the laboratory from measurements on submeter-sized specimens. There, unlike in the field, individual factors can be controlled and varied in a systematic manner to determine their role, if any. Where appropriate, size is discussed.

Although several kinds of ice exist in nature (H_2O, NH_3, CO_2), this review focuses on water ice, specifically on polycrystals of the low-pressure variant that possesses the hexagonal crystal structure, denoted Ih. High-pressure ice, of which there are more than a dozen variants of different crystal structures and densities (Petrenko & Whitworth 1999), is beyond the scope of this review, as are low-pressure cubic ice and amorphous ice.

Under terrestrial conditions, polycrystals of ice Ih exhibit either a granular microstructure (e.g., icebergs) in which individual grains typically of size 1 to 10 mm are equiaxed and randomly oriented or a columnar microstructure (e.g., sea ice) in which the crystallographic c axes of the individual grains, again typically 1 to 10 mm in diameter, exhibit a preferred orientation, often confined to and randomly oriented within the horizontal plane. Granular ice is mechanically isotropic. Columnar ice is orthotropic, and so its properties, as discussed elsewhere (Schulson & Duval 2009), must be viewed with respect to its microstructure and to the applied stress tensor. Little is known of the microstructure of extraterrestrial ice.

As will become apparent, experiments on water ice have elucidated not only the brittle failure of that material but also the behavior of rock and minerals.

Owing to space limitations, many details are omitted here. Also, equations (where necessary) are embodied in the lines of text but not derived. Details and derivations may be found in the literature cited.

2. INELASTIC BEHAVIOR: OVERVIEW

Ice exhibits two kinds of inelastic behavior. When strained slowly, it flows. Strains in excess of unity can be imparted without macroscopic failure, and the deformation is characterized by strain-rate hardening. Such behavior is termed ductile and is displayed, for instance, by temperate glaciers deforming under the influence of gravitational forces. When strained rapidly, however, ice behaves in a brittle manner: Fracture occurs suddenly after little inelastic deformation and results in either partial or complete loss of load-bearing ability. The kind of behavior and the transition from one kind to the other depend upon the combination of environmental (temperature, loading rate, stress state) and microstructural (porosity, grain size, salinity, crystallographic texture) factors.

Ductile behavior originates principally from crystallographic slip on basal planes, generally through the glide of dislocations of $a/3 < 11\bar{2}0 >$ Burgers vector. Under the combination of low stress ($<10^{-4}$ of the shear modulus), high temperature, and fine grain size (<0.1 mm), diffusion creep can contribute plastic strain. Plastic deformation is thermally activated, and the flow strength σ_D under an applied strain rate $\dot{\varepsilon}$ may be described by the relationship $\sigma_D = B^{-1/n}\dot{\varepsilon}^{1/n}$, where n is a materials constant, typically of value $n = 3$, and the parameter B increases with increasing temperature according to the relationship $B = B_o \exp(-Q/RT)$, where B_o is another materials constant, Q denotes activation energy, R is the universal gas constant, and T is absolute temperature.

Brittle behavior, in comparison, originates from the initiation, growth, and interaction of cracks. Correspondingly, the brittle failure strength σ_B may be described generally by the

relationship $\sigma_B = CK_{Ic}l^{-1/2}$, where K_{Ic} denotes the plane strain fracture toughness (described in Section 3), l is crack length, and the parameter C incorporates stress state and friction (Section 4.3). An exception is finely grained ice loaded under tension where the strength is controlled by crack nucleation (Lee & Schulson 1988). Brittle behavior persists right up to the point of melting, owing to a combination of sluggish dislocation kinetics and low resistance to crack propagation.

The transition from ductile to brittle (DB) behavior is caused by competition between stress buildup and stress relaxation at crack tips. It is not directly related to the appearance of microcracks, as bodies initially free from cracks can become riddled with nonpropagating cracks and yet exhibit macroscopically ductile behavior. As modeled elsewhere (Schulson 1990, Renshaw & Schulson 2001), the DB transition may be expressed in terms of a transition strain rate $\dot{\varepsilon}_{DB}$ described by a relationship of the form $\dot{\varepsilon}_{DB} = BC^n K_{Ic}^n l^{-n/2}$. The creepier and tougher the ice and the smaller the stress-concentrating cracks, the higher the transition strain rate. For granular ice and for columnar ice loaded across the columns, the transition strain rate at −10°C, for instance, is $\dot{\varepsilon}_{DB} \sim 10^{-8}$ to 10^{-7} s^{-1} under tension and between 10^{-4} and 10^{-3} s^{-1} under uniaxial compression. Within the ice cover on the Arctic Ocean where global inelastic deformation occurs intermittently and predominantly under far-field compression, the transition also occurs at a strain rate of around 10^{-4} s^{-1} when account is taken of the localized, spatiotemporal character of the process (Marsan et al. 2004, Schulson 2004, Rampal et al. 2008, Weiss & Dansereau 2017).

Readers interested in ductile behavior/creep may wish to consult reviews by Weertman (1983), Duval et al. (1983), Durham et al. (1997), Durham & Stern (2001), and Schulson & Duval (2009), and references therein.

3. FRACTURE TOUGHNESS

Plane strain fracture toughness is fundamental to brittle failure. The property is a measure of crack tolerance or of resistance to crack growth in the absence of significant expenditure of energy through plastic work and stems conceptually from linear elastic fracture mechanics. It specifies the critical value of the crack-opening or mode-I stress intensity factor K_I. Correct measurement requires that crack-tip creep be suppressed and, thus, that the rate of increase of $\dot{K}_I$ be sufficiently high, i.e., $\dot{K}_I > 0.002$ MPa $m^{1/2} s^{-1}$ at −10°C (Nixon & Schulson 1988); a higher rate is needed for warmer ice (Gharamti et al. 2021b) and for salty ice (see Schulson & Duval 2009, table 9.1). A good value of fracture toughness for pristine, terrestrial ice of ∼3-mm grain size is $K_{Ic} = 0.1$ MPa $m^{1/2}$ for both submeter- and suprameter-sized bodies (Schulson & Duval 2009, Gharamti et al. 2021b). Fracture toughness increases slightly with decreasing temperature, reaching $K_{Ic} = 0.14$ MPa $m^{1/2}$ at −173°C (Litwin et al. 2012). A distribution of fine (0.25 μm) particles of silica toughens ice by an amount that scales approximately with the square root of volume fraction, f, at least up to $f = 0.34$ (Yasui et al. 2017). Similarly, the eutectic mixture ice-$MgSO_4{\cdot}11H_2O$ increases fracture toughness by about 30% (Golding et al. 2013). Porosity, on the other hand, lowers crack tolerance by about 50% for $p = 0.4$ (Rist et al. 1999), owing to its effect on Young's modulus (Snyder et al. 2017). Cyclic loading has little detectable effect (Gharamti et al. 2021a).

Fracture toughness is related to materials toughness, G_c, through the relationship $G_c = K_{Ic}^2(1 - \upsilon^2)/E$. Poisson's ratio $\upsilon = 0.33$ and Young's modulus $E = 9.3$ GPa (Gammon et al. 1983) under terrestrial conditions, giving $G_c = 1$ J m^{-2}. This is several times the surface energy of ice, implying that the propagation of cracks, even under rapid loading, is not a purely elastic process. Grain boundaries may account for part of the difference, given that fracture toughness increases by about 30% as grain size decreases from 10 mm to 1 mm (Nixon & Schulson 1988). The other contributor may be crack-path tortuosity.

Of growing interest is the fracture toughness of sintered microspheres. This is of relevance to the future sampling of cold ice from Saturn's satellite Enceladus (Choukroun et al. 2020) where

micrometer-sized particles form following the intermittent emission of water-rich plumes from tiger stripe rifts in the south polar region (Hansen et al. 2006, Porco et al. 2017, Postberg et al. 2011) that then rain down, sintering over time (Molaro et al. 2019). To be determined, and elucidated perhaps from studies of snow (Kirchner et al. 2000, Schweizer et al. 2004), is the degree needed to impart significant toughness.

Ice is a fragile material. Its fracture toughness is lower than that of granite by more than an order of magnitude (Wang & Hu 2017), lower than glass by a factor of five or more (Varshneya 2006), and even lower than eggshells (Taylor et al. 2016) by about a factor of three. Its fragility, like its low melting point, originates from weak (∼0.7 eV/molecule) intermolecular hydrogen bonding. Yet, in the form of icebergs and floating ice sheets, it can exert large forces, toppling lighthouses, crushing ships, and transforming level ice into a field of rubble (Schulson & Duval 2009).

4. BRITTLE FAILURE

As already noted, the brittle failure strength generally scales as $\sigma_B \propto K_{Ic} l^{-1/2}$. In pristine ice the size of cracks that nucleate under load scales directly with grain size d (Cole 1988, Lee & Schulson 1988). This leads to both tensile and compressive strength scaling as $\sigma_B \propto d^{-1/2}$. The tensile strength of terrestrial ice is of the order of 1 MPa: It increases moderately with decreasing temperature, in proportion to the increase in fracture toughness (Litwin et al. 2012), and decreases with increasing salinity (Richter-Menge & Jones 1993). The unconfined compressive strength is higher, of the order of 5 to 10 MPa at −10°C, and increases quite markedly with decreasing temperature, reaching ∼70 MPa at −170°C (Arakawa & Maeno 1997). The difference between tensile and compressive failure reflects the role of frictional sliding under compression (Section 4.3).

4.1. Brittle Tensile Failure

Tensile failure occurs trans-granularly, through the operation of mechanisms reviewed earlier (Schulson & Duval 2009). With the exception of measurements on cold ice (Litwin et al. 2012), little has appeared within the past decade to expand the picture. Known earlier, but still unexplored, is a kind of superplasticity (Schulson & Kuehn 1993, Kuehn & Schulson 1994) imparted through deformation processing. The capacity for tensile elongation of up to 50% or more can be imparted to freshwater ice by slowly compressing warm ice a small percentage to initiate both recrystallization and the formation of a network of short cracks oriented along the direction of shortening. The underlying mechanism remains to be elucidated, although grain boundary sliding and cracks stopping cracks may contribute. Whether ductility of similar magnitude could be realized in nature should ice be loaded through a combination of slow compression-cum-rapid tension is not known.

An intriguing quality of ice is the ability to extend elastically to almost the theoretical limit without breaking (Xu et al. 2021). Ordinarily, ice breaks in two if extended less than 0.1% at strain rates greater than $\dot{\varepsilon}_{DB}$. However, in the form of fibers a few micrometers or less in diameter, processed using the method of electric-field enhanced growth (Ma et al. 2020), the material can be reversibly bent into a near-circular shape tens of micrometers in radius and then spring back with no residual curvature. In this manner, Xu et al. (2021) imparted an elastic extension of ∼11% and a corresponding stress of ∼1,400 MPa to the tensile surface of a cold (−150°C) microfiber. The extraordinary elasticity and strength is attributed to the absence of defects—cracks, grain boundaries, and dislocations—and to a smooth surface. Perhaps similar properties might be imparted to other nominally brittle materials through appropriate processing.

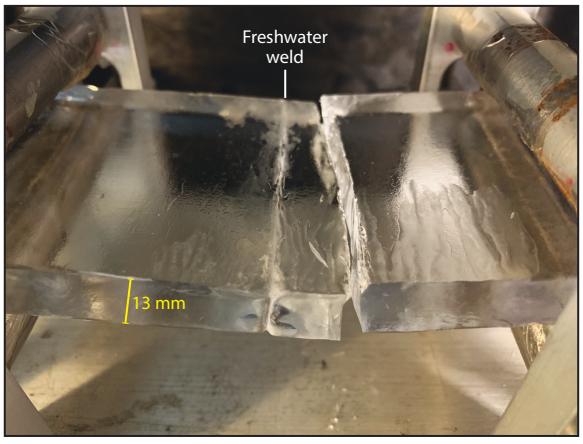

Figure 1

Photograph of a welded plate of columnar grained, freshwater ice bent to failure under 4-point loading at −10°C at an outer-fiber strain rate of $\sim 10^{-4}$ s^{-1}. The plate had been previously cut into two pieces and then welded back together with freshwater. The weld is shown as the whitish line in the image to the left of the fracture. Note that the fracture passed through the ice of the parent plate, not through the weld. The long axis of the grains is perpendicular to the large faces. Photo courtesy of Andrii Murdza.

4.2. Flexural Strength, Cyclic Hardening, Recovery, and Healing

Flexural strength is related to tensile strength, although it is greater by a factor of about 1.7. The flexural strength of warm ice can be increased by more than a factor of two through slow, reverse cycling (0.1 to 10 Hz) at progressively higher outer-fiber stresses (Iliescu et al. 2017; Murdza et al. 2020, 2021a,c). Evidence of cyclic strengthening has been obtained as well through direct tension-compression experiments (Cole 1995), and a hint (our word) of the effect may be seen in Brazil tests (Hammond et al. 2018). The added strength can be eliminated upon annealing (Murdza et al. 2022). Cyclic strengthening is attributed to the development through either dislocation pileups or grain boundary sliding of an internal back stress that opposes the applied stress in nucleating cracks. Recovery is attributed to a thermally activated relaxation of that internal stress. A consequence of this behavior is an apparent resilience against fatigue (Hammond et al. 2018, Murdza et al. 2020).

When flexed to failure and then welded together with either fresh- or salty water, the reassembled aggregate can heal, often failing in bending not through the weld but through adjacent material (Murdza et al. 2021b) (**Figure 1**). The weld, it seems, even when decorated with stress-concentrating pores, can be stronger than the parent material, owing, presumably, to a microstructure different from the parent ice. In the absence of water, when surfaces of ice are pushed together, healing ensues and strength is restored (Schulson et al. 2016).

4.3. Brittle Compressive Failure: Coulombic Faulting

Brittle failure under compression is more complicated. It is best viewed more as a process than as an event. The unique combination of large grain size and optical transparency of freshwater ice as well as the experimental ability to keep constant during loading the degree of triaxiality of the stress state has allowed details of the process to be revealed to the unaided eye. In addition to crack nucleation and propagation, coming into play are stable crack growth, crack interaction, and the development of a culminating macroscopic fault. Again, the details were reviewed earlier

(Schulson & Duval 2009), and little has appeared during the past decade to expand the picture—except of brittle-like failure (Section 4.4).

To summarize brittle compressive failure per se, at root is the frictional-sliding wing-crack mechanism of Griffith (1925), McClintock & Walsh (1962), Ashby & Hallam (1986), and Horii & Nemat-Nasser (1986) and the comb-crack derivative thereof (Schulson et al. 1999, Renshaw & Schulson 2001). Accordingly, and as first reported by Cannon et al. (1990), sliding under uniaxial loading occurs across the opposing faces of closed, parent/primary cracks, either preexisting or nucleated during loading, once the effective shear stress resolved onto the plane of the cracks, τ_{eff}, overcomes frictional resistance. Sliding induces at the crack tips tensile stress that, when sufficiently high, is relieved through the initiation of out-of-plane secondary cracks, termed wings (or extensile cracks), oriented along the direction of loading. Tension is then concentrated at the tips of the wings. As load increases, sliding continues and the wings open; also, more primary cracks nucleate. If sliding speed, $\dot{u}$, is high enough, set by the applied strain rate and grain size ($\dot{u} \propto \dot{\varepsilon} d$), K_{I} reaches K_{Ic} and the wings begin to lengthen in a stable, albeit jerky, manner. When sliding is too slow, stress relaxes at the wing tips, in which case ductile behavior ensues. Wing cracks interact as they lengthen, leading under uniaxial loading to the initiation and length-wise growth of one or more macroscopic splits that culminate in terminal failure. Confinement lowers K_{I} and reduces τ_{eff}, thereby raising quite markedly the applied stress needed to activate the process. Also, even at a very low level (Wachter et al. 2009), confinement changes the mode of terminal failure, from axial splitting to shear faulting, owing to the onset of splay-like comb cracking. The faults often form conjugate sets and are inclined to the direction of shortening by an angle θ, set by the coefficient of kinetic friction μ_{k} and given by the relationship $\tan 2\theta = 1/\mu_{\text{k}}$ (Jaeger & Cook 1979, Schulson & Duval 2009). Under terrestrial conditions $\theta \sim 30°$, implying that $\mu_{\text{k}} \sim 0.6$. Such faults are termed Coulombic (C) faults.

Modeling on the basis of the wing crack-cum-comb crack mechanism leads to the brittle compressive strength being expressed in terms of not only fracture toughness and crack size but also the coefficient of kinetic friction and the degree of confinement. Included is sliding across the free ends of the slender, fixed-free microplates (like a sliding thumb across the teeth of a comb) that form on one side of the primary crack through nonuniform sliding. The model has no adjustable parameters and, as shown by the nondimensionalized (with respect to crack length and fracture toughness) calculations in **Figure 2**, accounts reasonably well for the brittle compressive strength of ice. The model also accounts for the brittle compressive strength of rock and minerals (Renshaw & Schulson 2001).

4.4. Brittle-Like Compressive Failure: Plastic Faulting

A different kind of failure occurs under high confinement. Whether warm or cold, pure or salty, granular or columnar, ice exhibits brittle-like behavior when rapidly compressed under a relatively high degree of triaxial confinement (Durham et al. 1983; Schulson 2002; Golding et al. 2010, 2012, 2014, 2020; Renshaw & Schulson 2017). The failure is brittle like in the sense of the sudden loss of load-bearing ability following a pseudolinear increase in applied stress and the attendant development of a fault. The high-confinement failure, however, is less noisy, and the faults form on planes inclined not by ~30° to the direction of shortening but by ~45°, i.e., on planes of maximum applied shear stress. Both low- and high-confinement faults localize inelastic strain into narrow [O (mm)] bands, but of different structure and properties: Microcracks and loss of cohesion develop under low confinement versus recrystallization and retention of cohesion under high confinement. Localization of strain raises temperature in both cases, but by an order of magnitude greater (i.e., by ~3°C) within high-confinement faults (Golding et al. 2010). The other difference

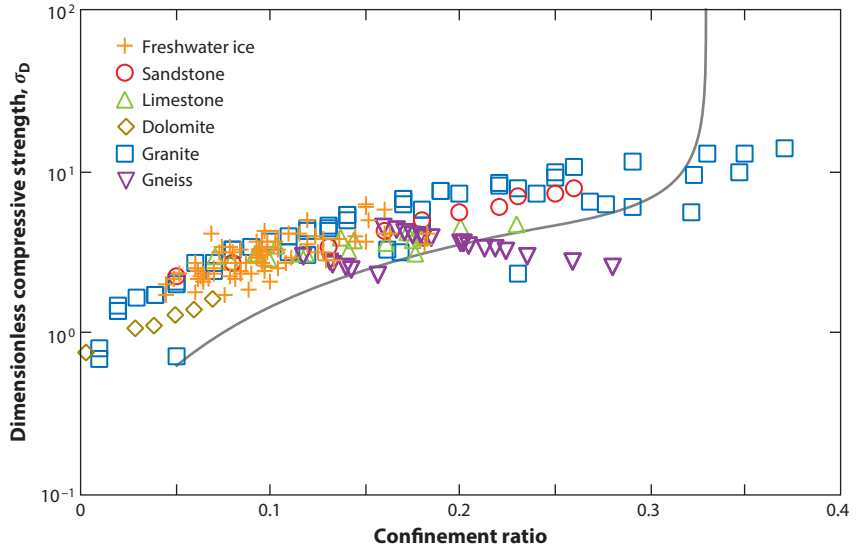

Figure 2

Brittle compressive strength (nondimensionalized) of ice and of a variety of rocks and minerals versus degree of confinement. The gray curve through the data was computed based upon the comb-crack model of frictional sliding. The curve turns sharply upward as confinement suppresses sliding. Figure adapted with permission from Renshaw & Schulson (2001).

is that the failure strength under high confinement is insensitive to both grain size and pressure. These differences imply that faulting under high confinement originates not from cracking and frictional sliding but from a volume-conserving, nonfrictional process involving crystallographic slip. For that reason, the faults are termed plastic or P faults and are viewed as physically distinct from low-confinement C faults. **Figure 3** shows both kinds plus the C → P transition and related stress-time curves.

P faults form when the hydrostatic component of the stress tensor is sufficient to suppress frictional sliding, while the deviatoric component remains nonzero. Inelastic deformation then occurs via dislocation glide. Under high strain rates, plastic strain is imparted adiabatically, as described elsewhere (Frost & Ashby 1982, Schulson 2002, Golding et al. 2010, Renshaw & Schulson 2017), leading to thermal softening, which overcomes both strain and strain-rate hardening, and to an increase in localized plastic flow. Ultimately, a P fault develops. The transition from C faulting to P faulting occurs when the degree of confinement reaches a critical level, $\chi = \chi_t$, given by the relationship (Schulson 2002, Golding et al. 2010) $\chi_t = [(\mu_k^2 + 1)^{1/2} + \mu_k]^{-2}$. [Whereas triaxial confinement of granular ice is defined simply as the ratio of the least to the greatest compressive stress, the definition for columnar ice must take into account the grain structure and is given by Golding et al. (2010).] For $\mu_k \sim 0.5$ to 0.6, $\chi_t \sim 0.3$ to 0.4, in good agreement with observation (see **Figure 3**).

Brittle-like failure is not limited to ice. It operates, for instance, within antigorite when the strain rate within an incipient adiabatic instability increases to the point that the attendant increase in localized temperature approaches a phase transition (Renshaw & Schulson 2017). Similarly, narrow, high-angle P faults have been observed in granite (Tullis & Yund 1977, Shimada 1992) and in olivine (Schubnel et al. 2013). Perhaps this mode of compressive failure limits the strength of all rock and minerals when rapidly loaded under high triaxial confinement and plays a significant role in the development of deep earthquakes.

5. FRICTION

As already noted, friction plays an important role in brittle compressive failure, certainly on the smaller scale of sliding across the faces of microcracks. On the larger scale of the winter cover on

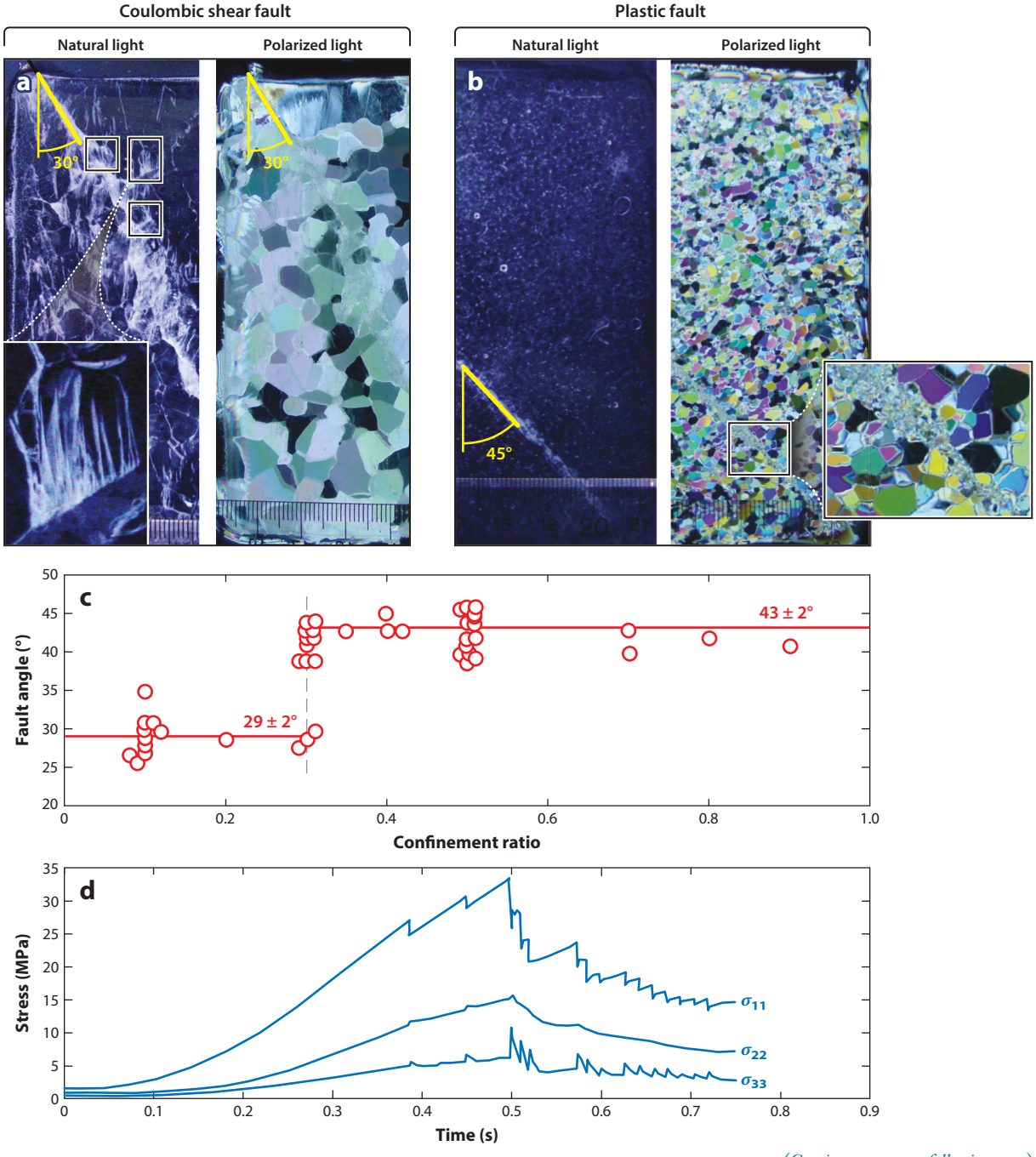

(*Caption appears on following page*)

Figure 3 (*Figure appears on preceding page*)

(*a*) Photographs of a typical thin (~1 mm) section of a Coulombic shear fault formed in freshwater, granular ice under a low degree ($\chi = 0.2$) of triaxial confinement, seen under natural (*left*) and polarized (*right*) lighting. The larger grain size allows the microstructure of comb cracks (*highlighted*) to be seen. The direction of shortening is vertical in the image. The smallest distance is 1 mm. The inserts show comb cracks. (*b*) Photographs of a typical thin section of a plastic (P) fault formed in the same kind of ice under a high degree ($\chi = 0.5$) of triaxial confinement, seen under natural (*left*) and polarized (*right*) lighting. Note the higher angle (45° versus 30°) of the P fault and the absence of microcracks. The highlighted regions show recrystallized grains along the fault. The smallest distance is 1 mm. (*c*) Summary of measured fault angles (with respect to direction of shortening at −10°C) versus degree of triaxial confinement. The dashed gray line indicates confinement at which frictional sliding is suppressed for $\mu_k = 0.6$, computed from the model in the text. (*d*) Representative plots of principal stresses versus time showing partial drops in stress during brittle-like compressive failure in columnar freshwater ice rapidly loaded at $\dot{\varepsilon}_{11} = 3 \times 10^{-2}$ s^{-1} at −10°C under a degree of triaxial confinement high enough to suppress frictional sliding and activate P faulting. Figure adapted with permission from Golding et al. (2010, 2012) and Renshaw & Schulson (2017).

the Arctic Ocean (Marko & Thomson 1977, Hibler & Schulson 2000, Schulson 2004, Schreyer et al. 2006, Weiss et al. 2007, Wilchinsky & Feltham 2011), the Antarctic ice sheet (Tsai et al. 2015, McCarthy et al. 2017), the tiger stripe rifts on Enceladus (Smith-Konter & Pappalardo 2008, Olgin et al. 2011), and the strike-slip faults on Europa (Hoppa et al. 1999), friction also affects the mechanics of deformation. Of interest, therefore, are the coefficients of static and kinetic (dynamic) friction.

5.1. Static Friction

The coefficient of static friction increases the longer a load is applied before sliding. Slide-hold-slide experiments, whether performed in the field (Pritchard et al. 2012, Sukhorokov & Loset 2013, Scourfield et al. 2015), in an ice tank (Lishman et al. 2011), or in the lab (Schulson & Fortt 2012, 2013), have revealed that the coefficient of static friction, defined as $\mu_s \triangleq F_s/F_n$, where F_s and F_n, respectively, denote shear load and normal load acting on an interface at the onset of sliding, increases with the logarithm of holding time, t_h (**Figure 4**). The effect, termed static strengthening, is described by the relationship $\mu_s = \mu_{os} + \beta \log_{10} t_h$, where μ_{os} denotes a reference coefficient. For ice on ice, the coefficient β decreases with decreasing temperature, from $\beta = 0.3$ at ~−10°C to $\beta \sim 0.1$ at −75°C to $\beta < 0.03$ at −100°C and −175°C for hold times up to 3 h. For warm ice

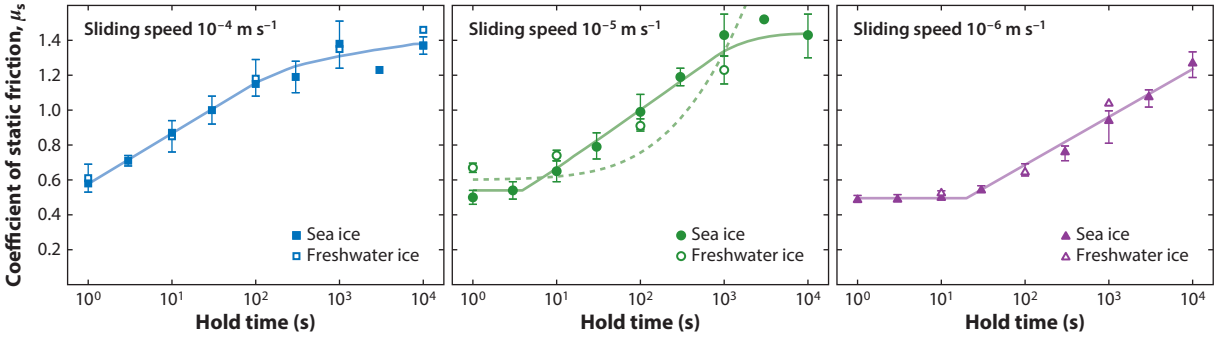

Figure 4

Coefficient of static friction of ice on ice, μ_s, versus hold time for both granular freshwater ice and first-year columnar sea ice, derived from slide-hold-slide tests at −10°C at sliding speeds of 10^{-6}, 10^{-5}, and 10^{-4} m s^{-1}. The dashed curve in the central panel was calculated from the model presented in the text. Note that following a threshold period, static friction increases linearly with the logarithm of hold time up to some limit and the threshold period increases with decreasing sliding speed. Note also that within the scatter in the measurements, shown by the short vertical bars through the means, sea ice cannot be distinguished from freshwater ice. Figure adapted with permission from Schulson & Fortt (2013).

on granite, $\beta \sim 0.1$ (McCarthy et al. 2017). The presence of brine pockets in sea ice has no detectable effect (Schulson & Fortt 2013), nor does the presence of saltwater external to the sliding interface (Sukhorokov & Loset 2013). Static strengthening also characterizes a variety of non-icy materials, including rock (Dieterich 1978, Marone 1998), metals (Dokos 1946), and glassy polymers (Berthoud et al. 1999) where the strengthening coefficient β is again lower than it is for warm ice on warm ice.

Friction originates from the interaction of asperities that protrude from opposing surfaces (Bowden & Tabor 1950, 1964). The effect of hold time on the coefficient of static friction can be understood in terms of a creep-driven increase in the true area of contact (a factor of 100 or more lower than the apparent area). Modeling in terms of adhesion and power-law creep leads to the relationship for warm (−10°C) ice $\mu_s = 0.6(1 + 0.01t_h)^{1/3}$ for hold time in seconds (Schulson & Fortt 2013). This is shown by the dashed curve in **Figure 4** and agrees reasonably well with measurement. (Logarithmic character can be captured by invoking logarithmic creep instead of power-law creep.)

Implicit in the model is asperity size. Its average value may be derived (Schulson & Fortt 2013) by equating the total interaction time to the sum of the holding time plus the time for asperities to slip past each other and then by assuming that holding begins to exert a detectable effect when the slip time equals the threshold time for detecting an effect. The analysis for ice gives an average diameter of 30 μm. This is about a factor of three smaller than the size of brine pockets in sea ice and of the spacing between them, implying that asperities in that material are essentially composed of freshwater ice, thereby accounting for the absence of an effect of salinity on the coefficient of static friction. The asperity size derived for ice is within the range (1 to 100 μm) derived for other materials (Persson 2000).

5.2. Kinetic Friction

Once initiated, sliding continues with lower resistance, albeit in a stick-slip manner. Under moderate (<2 MPa) normal stresses and over a wide range of temperatures (−175 to −10°C), ice obeys Coulomb's law $\tau_s = \tau_o + \mu_k\sigma_n$, where the coefficient of kinetic friction, μ_k, is defined as the derivative of the shear stress, τ_s, with respect to the normal stress, σ_n; cohesion, τ_o, tends to be low, and so the coefficient derived simply from the ratio τ_s/σ_n does not overly exaggerate its value (Schulson & Fortt 2012). The kinetic coefficient exhibits no detectable sensitivity to grain size, to crystallographic texture, to both internal and external saltwater, to sliding direction, and to sliding distance (at least up to 20 mm), but it is affected by roughness and by the presence of the hydrated salt $MgSO_4$. Most importantly, the coefficient is sensitive to sliding speed and to temperature.

At speeds lower than $V_s \sim 10^{-4}$ m s^{-1} the kinetic coefficient for warm ice increases slightly with increasing velocity, while at speeds above some transition velocity, V_t, the coefficient decreases (**Figure 5**). (At still higher speeds, frictional heating melts the interface and hydrodynamic sliding—which is beyond the scope of this review—sets in.) The effect of temperature is less systematic, from a monotonic increase with decreasing temperature at higher velocities (Schulson & Fortt 2012, McCarthy et al. 2017) to mixed dependence at lower speeds. The coefficient appears to scale with roughness ρ as $\mu_k \propto \rho^{0.08}$ and $\mu_k \propto \rho^{0.3}$ within the strengthening and weakening regimes, respectively. An implication of the dual effect of velocity is that sliding within natural bodies, such as the ice cover on the Arctic Ocean, may become unstable once sliding speed exceeds the transition velocity.

The interaction of asperities is again at root. At the lowest speeds, the time for asperities to slide past each other is long enough to allow frictional heat to be conducted away. As a result, contacts remain dry and asperities deform by creeping under an effective shear stress. Strain-rate

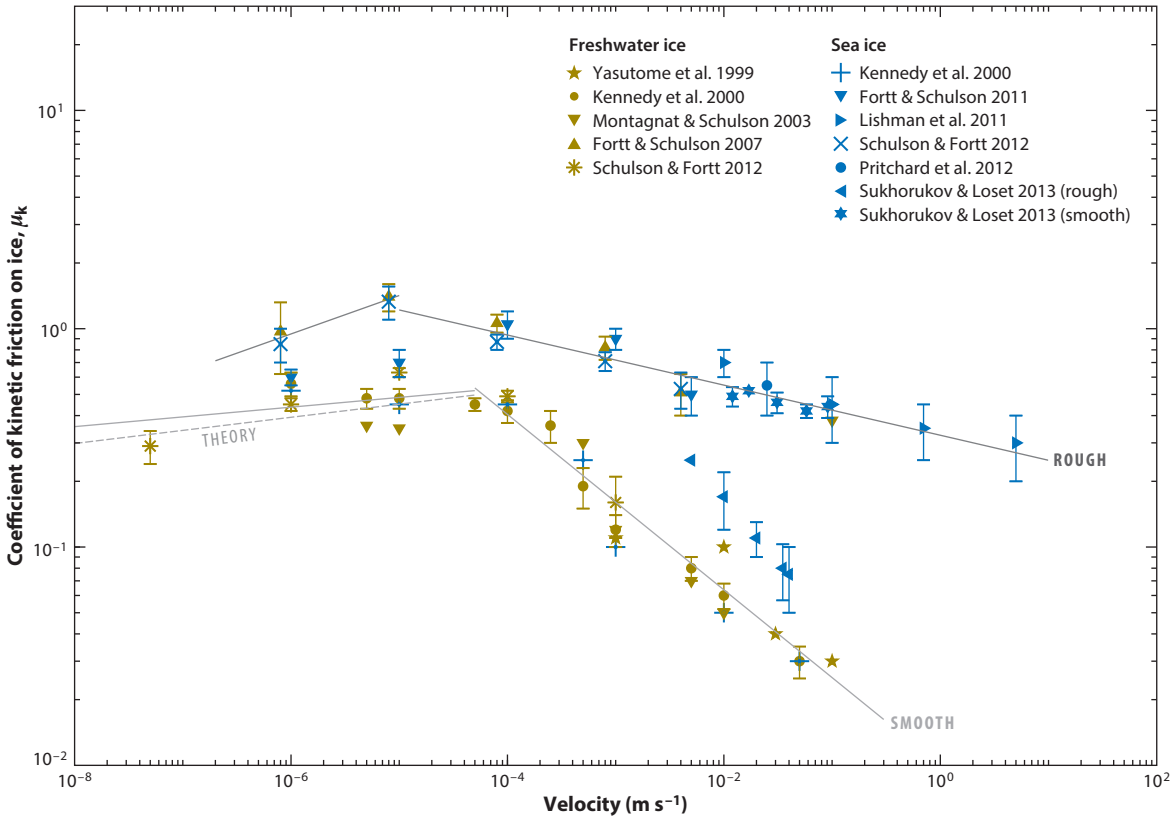

Figure 5

Coefficient of kinetic (dynamic) friction of ice on ice, μ_k, versus sliding velocity for both freshwater ice (*brown points*) and sea ice (*blue points*). The dashed curve over the range of lower velocities was computed from the equation in the text. Figure adapted with permission from Schulson (2018).

hardening, and hence velocity strengthening, ensues. However, as the velocity reaches a certain level, the smallest contacts begin to melt. The attendant lubrication counteracts strain-rate hardening and leads to the onset of velocity weakening. Beyond that point progressively larger asperities melt, leading to an increasing fraction of wet contacts, further lubrication, and further weakening. At still-higher velocities, all contacts melt, at which point hydrodynamics sets in.

Velocity strengthening (i.e., dry sliding) has been modeled (Schulson 2015, 2018) in terms of the ratio of the shear strength and the hardness of asperities. Both properties are thermally activated (Barnes et al. 1971). Modeling for warm ice (−10°C) leads to the relationship $\mu_{kd} = 0.9V_s^{0.07}$ for velocity in meters per second, shown by the dashed line in **Figure 5** and in good accord with measurement. That saline ice and freshwater ice are practically indistinguishable is again taken to mean that asperities in both materials comprise essentially pure ice.

Velocity weakening sets in when time is insufficient to allow frictional heat to be conducted away through opposing interfaces. The transition velocity, V_t, is found from a one-dimensional heat-transfer analysis (Schulson 2015) to scale as $V_t \propto a\Delta T^2$, where a denotes asperity size and ΔT denotes the difference in temperature between the contact and the bulk of the ice. An implication is that cold ice sliding slowly may not exhibit velocity weakening, in keeping with observation (Schulson & Fortt 2012).

At speeds above the transition velocity but below the onset of all-hydrodynamic sliding, a mix of dry (larger contacts) and wet (smaller contacts) is envisaged. The coefficient of kinetic friction may then be described by a rule of mixtures $\mu_k = \mu_{kd}(1 - \eta) + \mu_w\eta$, where η denotes the fraction of the real area of contact covered by a thin layer of meltwater and μ_w is the coefficient of kinetic friction of water. The parameter η has been quantified in terms of the transition and the sliding velocities by assuming that asperities exhibit fractal character and that $\mu_w \sim 0$. This leads to the relationship (Schulson 2018) $\mu_k = \mu_{kd}(1 - FS(V_s^{4-2D} - V_t^{4-2D})/A_o(2 - D))$, where F is a function of several parameters (thermal conductivity, density, specific heat, latent heat of fusion, thickness of water layer, and ΔT), A_o denotes the initial real contact area, and S and D characterize the distribution of contact areas $dN(A)/dA = S/A^D$, where $N(A)$ is the total number of contacts of area equal to or smaller than A. Although S and D are not known for ice, analysis of the data in **Figure 5** in terms of the fractal model (Schulson 2018) leads to the value $D = 1.90 \pm 0.05$. This value is comparable to D values measured from contact surfaces on quartz, calcite, and glass (Dieterich & Kilgore 1996).

A different interpretation of low-speed friction is based on thermodynamics (Makkonen 2012, Makkonen & Tikanmaki 2014). The idea is that sliding is resisted by the surface energy, ψ, of newly created steps and ledges of nanoscale dimensions. Accordingly, $\mu_k = \psi/H\lambda$, where H denotes hardness and λ is the size of the smallest cluster of H_2O molecules in ice. Taking $\psi = 0.075$ J m^{-2}, $\lambda = 2$ nanometers, and $H = 60$ MPa at -10°C leads to the value $\mu_k = 0.6$ for dry sliding in warm ice, in good agreement with measurement. The problem is that owing to an increase in hardness with decreasing contact time (Barnes et al. 1971) and hence increasing sliding velocity, the thermodynamic model dictates an effect of velocity on dry sliding opposite to the one observed. This is not to say that the creation of new surface does not contribute to sliding resistance, but that its contribution may be less than imagined.

Dual behavior, from strengthening to weakening with increasing velocity, is exhibited by several other icy systems as well, including warm ice on granite and on glass (Barnes et al. 1971). Rock on rock (Chester 1988, Reinen et al. 1992, Kilgore et al. 1993, Noda & Shimamoto 2010) shows the same character. Ice on steel, on concrete, on rubber, and on nylon (Saeki et al. 1986, Akkok et al. 1987, Kietzig et al. 2010) exhibit velocity weakening at speeds above $\sim 10^{-4}$ m s^{-1}. In other words, dual behavior may be a general characteristic of low-speed, frictional sliding of multicontact material systems in which low thermal conductivity of at least one component offers the potential for a phase transformation through frictional heating.

There is no evidence that size affects the coefficient of kinetic friction. The friction-controlled slope of the low-confinement branch of the brittle compressive failure envelope is essentially the same for both submeter specimens of ice and kilometer-sized sea ice floes (Weiss et al. 2007), and the friction-controlled included angle between conjugate sets of Coulombic shear faults in submeter-sized specimens is almost the same as the included angle between sliding linear-kinematic features [taken to be large-scale strike-slip faults (Marko & Thomson 1977, Schulson 2004)]. These two observations, limited although they are, suggest that friction of ice is independent of spatial scale. This apparent independence on size is a reflection, perhaps, of the fact that resistance to sliding originates from the interaction of asperities that are fractal in character where smaller asperities are superimposed upon larger asperities at all spatial scales.

6. PERMEABILITY

In recent years, the permeability of ice has received increasing attention and, as already noted, cracks play a role. During peak sea ice melt season, ice permeability regulates the formation of melt ponds that alter the energy balance of the ice-ocean system by lowering the albedo, accelerating

melting (Curry et al. 1995, Perovich et al. 2002, Eicken et al. 2004, Serreze et al. 2009, Flocco et al. 2010, Polashenski et al. 2012), and increasing the availability of light for primary productivity beneath the ice by reducing the backscattering of light from exposed ice (Frey et al. 2011, Arrigo et al. 2012, Nicolaus et al. 2012). In freshwater ice, the permeability of firn allows surface meltwater to infiltrate and warm subsurface firn, creating perennial firn aquifers (e.g., Forster et al. 2014, Miege et al. 2016, Miller et al. 2020). Elsewhere, the sudden onset of percolation below supraglacial lakes can deliver large volumes of water to the bed, reducing basal traction (Zwally et al. 2002, Das et al. 2008, Andrews et al. 2018, Chudley et al. 2019). In some cases, reduced basal tractions drive transient ice-sheet acceleration that triggers additional lake drainage (Stevens et al. 2015, Christoffersen et al. 2018). Where cracking acts is detailed in Sections 6.1 and 6.2.

6.1. Sea Ice

Most experimental laboratory studies of ice have focused on variations with temperature in the permeability of columnar, saline ice (Ono & Kasai 1985, Kawamura et al. 2006, Golden et al. 2007, Pringle et al. 2009). These laboratory studies have been complemented by several notable field studies that also address the variation in sea ice permeability with temperature (Golden 2001, Eicken et al. 2002, Freitag & Eicken 2003, Polashenski et al. 2017). Much of this work was motivated by the observation that sea ice is effectively impermeable for porosities less than about 5% (Weeks & Ackley1986). Saline ice porosity is directly related to temperature (Frankenstein & Garner1967): As the temperature of sea ice rises, the volume of brine pockets, and hence porosity, grows to maintain their salinity at the freezing point. When the porosity increases beyond a critical threshold [about 5% for columnar first year ice (Golden et al. 1998)], both percolation theory and experimental observations indicate that percolation onsets as the pores form a connected pathway through the ice. In the field, however, infiltrating freshwater from melting snow can freeze and block pathways, sealing the ice against percolation. Given sufficient snow, Polashenski et al. (2017) observed that percolation blockage limits sea ice permeability for ice temperatures less than ~1°C.

In addition to brine pockets and channels, cracks/fractures, at scales both large and small, are common in sea ice (Kwok 2001, Schulson 2004). Above a critical fracture density, cracks link together to create a continuous pathway for flow and thus can also contribute to the critical behavior of ice permeability (Renshaw 1999). Yet the impact of inelastic deformation on the permeability of ice has received less attention. Renshaw et al. (2018) observed that when confinement was sufficient to suppress frictional sliding, the applied compression closed cracks and brine channels, decreasing ice permeability, in some cases by orders of magnitude. A potentially important implication of this observation concerns wave-energy dissipation. When sufficiently permeable, the dissipation of wave energy is dominated by the migration of brine through the ice (Marchenko & Lishman 2017). However, above some critical wave amplitude, compression induced by bending might lower permeability to the point of inhibiting brine migration and, thus, of limiting wave-energy dissipation. An implication is an increase in coastal erosion.

It is likely that both cracks and brine channels contribute to sea ice permeability, with their relative contributions spanning a continuum across different conditions of temperature, salinity, wind stress, etc. Although systematic studies remain to be performed, Renshaw & Schulson (2017) sought to define the fracture end member of this continuum by investigating the role of strain in controlling crack-induced percolation in freshwater columnar ice—i.e., in ice free from brine channels. They found that the threshold for along-column permeability corresponds with the ductile peak compressive strength (~2 to 3 MPa for 3- to 8-mm columnar ice loaded across the columns) and that lateral connectivity only develops over a limited distance. Although in low-porosity freshwater, columnar ice, the applied stress corresponding to the onset of along-column

percolation is higher than measured stresses in sea ice (Richter-Menge et al. 2002), porous saline ice is softer and hence the threshold stress required to impart the critical strain for percolation is likely to be lower. The limited lateral connectivity of the flow networks probably contributes to the observation that the fraction of late-summer melt pond coverage is near the critical percolation threshold below which the ponds are largely disconnected (Popovic et al. 2020).

6.2. Glacier Ice

The idea that the rapid drainage of supraglacial lakes is due to the propagation of large (kilometer-scale length) hydro-fractures directly beneath the lake has received intense study (e.g., Das et al. 2008, Doyle et al. 2013, Stevens et al. 2015, Christoffersen et al. 2018), particularly as supraglacial lakes have become larger and more numerous and have expanded their range inland to higher elevations (Howat et al. 2013). While the basic principles of hydro-fracture through glacial ice are well understood (van der Veen 2007, Krawczynski 2009), the mechanism that initiates the hydro-fractures is less certain (Doyle et al. 2013) but may be related to increased lake volume reactivating preexisting fractures (Chudley et al. 2019) or surface stress perturbations related to hydrologically induced basal slip (Stevens et al. 2015, Christoffersen et al. 2018).

The scarcity of experimental laboratory studies of surface initiating hydraulic fractures reflects the logistical challenges in creating such cracks in laboratory samples. However, recent work on the cracking of granular ice (Renshaw et al. 2019, 2020) has revealed insight into how connected flow pathways are created. At relatively high strain rates that are still lower than the DB transitional strain rate (Schulson 1990, Renshaw & Schulson 2001), the strain at percolation is scale invariant, flow paths are distributed across the sample, and percolation occurs at crack densities similar to those predicted by percolation theory. Further, with additional strain the crack density remains nearly constant after the onset of percolation even while permeability increases, indicating that after the onset of percolation the increase in permeability is primarily due to the opening of existing cracks rather than the extension of cracks. Because after the onset of percolation additional strain does not impart additional crack growth, the effective elastic properties (e.g., Young's modulus) are mostly insensitive to postpercolation strain. An implication is that after the onset of percolation, measurements that reflect changes in effective elastic properties, such as seismic velocities, are likely insensitive to the evolving changes in permeability with additional strain.

At lower strain rates (e.g., lower than 10^{-5} s^{-1} in uniaxially compressed 1- to 2-mm grain-size freshwater, granular ice at −10°C), the percolation threshold is scale dependent and flow occurs mostly along a single flow pathway controlled by the longest cracks. That is, crack propagation at strain rates below a critical threshold is consistent with the idea of the onset of percolation being controlled by the growth of a small number of large cracks. Above this threshold strain rate, however, cracking is expected to be more distributed and so the onset of percolation results from the interconnection of many smaller cracks. Notably, measured surface strain rates near rapidly draining supraglacial lakes are of order 10^{-9} s^{-1} (Chudley et al. 2019)—i.e., within the regime where permeability is expected to be controlled by the growth of a few long cracks such as hydraulic fractures rather than the connection of many smaller cracks.

7. FUTURE WORK

In its multiple forms, from temperate glaciers to ice covers to icy crusts within the outer Solar System, water ice constitutes a major structural material within both terrestrial and extraterrestrial geophysical systems. It may be loaded either slowly or rapidly under a variety of stress states and may fail in either a brittle manner after little inelastic deformation or a ductile manner after extensive flow. We hope this review serves to describe recent progress on the character and

physics of brittle failure, friction and its role in brittle compressive failure, and crack-induced permeability. More work is needed, both to deepen the understanding of ice per se and—owing to its distinct experimental advantages, including simplified mineralogy, grain-size control, optical transparency, and easy sample preparation and disposal—to further elucidate the behavior of other natural materials.

7.1. Fatigue

The apparent resistance to fatigue failure of warm, pristine ice is rather surprising. Is the resistance only apparent, the real behavior hidden by the statistical character of the process and by the relatively few experiments to date? Or is the resistance a manifestation of some kind of dynamic crack healing? Does cold ice show similar resistance?

7.2. Fracture and Calving

To gain further insight into the underlying mechanisms, there is a pressing need for experimental studies, guided by fracture mechanics, to complement numerical simulations of calving glaciers.

7.3. Brittle and Brittle-Like Compressive Failure

The nature of C and P faulting in both warm and cold ice may be enlightened further by investigating the role of porosity and its distribution, taking cognizance of pore collapse and the crushing of ice adjacent to pore walls. Ice may well serve as a model for crustal rock.

7.4. Friction

The models of asperity interaction that have been proposed to account for the coefficients of static and kinetic friction are based predominantly upon supposition. To advance understanding, direct observations of sliding interfaces are needed, with attention to stick-slip, to spatiotemporal dynamics, and to possible rupture fronts (Svetlizky et al. 2019). A potential avenue for exploration might be to exploit the proposed fractal character of the interface and to investigate scaled models.

7.5. Failure of Cold, Salty Ice

In relation to extraterrestrial studies and to the mechanics of the icy crusts of a number of planetary satellites, work is needed on the mechanical properties of cold water ice enriched with NaCl, $MgSO_4$, and possibly other salts. In contrast to the more coarsely grained, fully dense ice studied to date, sintered microspheres and finely grained, porous material merit attention.

7.6. Failure of Healed Ice

While new damage in the form of microcracks is continually being imparted when ice is loaded under natural forcing, old damage is continually healing, lessening its weakening effect. Similarly, healed interfaces can, in some cases, be stronger than the original parent material, owing presumably to a different microstructure. Healing and interfacial strengthening remain to be systematically studied.

7.7. Permeability

Although significant progress has been made in understanding how cracks lead to the creation of new flow pathways to allow permeability, studies to date have been limited to ice with very

low porosity. Even in the absence of microfracturing, it is known that sufficient porosity per se can result in flow pathways. Additional work is needed to understand how fracture and porosity interact.

DISCLOSURE STATEMENT

The authors are not aware of any affiliations, memberships, funding, or financial holdings that might be perceived as affecting the objectivity of this review.

ACKNOWLEDGMENTS

The authors gratefully acknowledge the National Science Foundation for financial support through award 1947107.

LITERATURE CITED

Akkok M, Ettles CMM, Calabrese SJ. 1987. Parameters affecting the kinetic friction of ice. *J. Tribol.* 109:552–59

Andrews LC, Hoffman MJ, Neumann TA, Catania GA, Luthi MP, et al. 2018. Seasonal evolution of the subglacial hydrologic system modified by supraglacial lake drainage in western Greenland. *J. Geophys. Res. Earth Surf.* 123:1479–96

Arakawa M, Maeno N. 1997. Mechanical strength of polycrystalline ice under uniaxial compression. *Cold Reg. Sci. Technol.* 26:215–29

Arrigo KR, Perovich DK, Pickart RS, Brown ZW, van Dijken GL, et al. 2012. Massive phytoplankton blooms under Arctic sea ice. *Science* 336:1408

Ashby MF, Hallam SD. 1986. The failure of brittle solids containing small cracks under compressive stress states. *Acta Metall.* 34:497–510

Barnes P, Tabor D, Walker JCF. 1971. The friction and creep of polycrystalline ice. *Proc. R. Soc. A* 1557:127–55

Berthoud P, Baumberger T, G'Sell C, Hiver J-M. 1999. Physical analysis of the state- and rate-dependent friction law: static friction. *Phys. Rev. B* 59:14313–27

Bowden FP, Tabor D. 1950. *The Friction and Lubrication of Solids*. Oxford, UK: Clarendon

Bowden FP, Tabor D. 1964. *The Friction and Lubrication of Solids, Part II*. Oxford, UK: Clarendon

Cannon NP, Schulson EM, Smith TR, Frost HJ. 1990. Wing cracks and brittle compressive fracture. *Acta Metall. Mater.* 38:1955–62

Chester FM. 1988. The brittle-ductile transition in a deformation-mechanism map for halite. *Tectonophysics* 154:125–36

Choukroun M, Molaro JL, Hodyss R, Marteau E, Backes P, et al. 2020. Strength evolution of ice plume deposit analogs of Enceladus and Europa. *Geophys. Res. Lett.* 47:e2020GL088953

Christoffersen P, Bougamont M, Hubbard A, Doyle SH, Grigsby S, Pettersson R. 2018. Cascading lake drainage on the Greenland Ice Sheet triggered by tensile shock and fracture. *Nat. Commun.* 9:1064

Chudley TR, Christoffersen P, Doyle SH, Bougamont M, Schoonman CM, et al. 2019. Supraglacial lake drainage at a fast-flowing Greenlandic outlet glacier. *PNAS* 116:25468–77

Cole DM. 1988. Crack nucleation in polycrystalline ice. *Cold Reg. Sci. Technol.* 15:79–87

Cole DM. 1995. A model for the anelastic straining of saline ice subjected to cyclic loading. *Philos. Mag. A* 72:231–48

Curry JA, Schramm JL, Ebert EE. 1995. Sea-ice albedo climate feedback mechanism. *J. Clim.* 8:240–47

Das SB, Joughin I, Behn MD, Howat IM, King MA, et al. 2008. Fracture propagation to the base of the Greenland Ice Sheet during supraglacial lake drainage. *Science* 320:778–81

Dieterich JH. 1978. Time-dependent friction and the mechanics of stick-slip. *Pure Appl. Geophys.* 116:790–806

Dieterich JH, Kilgore BD. 1996. Imaging surface contacts: power law contact distributions and contact stresses in quartz, calcite, glass and acrylic plastic. *Tectonophysics* 256:219–39

Dokos SJ. 1946. Sliding friction under extreme pressures—1. *J. Appl. Mech.* 13:A148–56

Doyle SH, Hubbard AL, Dow CF, Jones GA, Fitzpatrick A, et al. 2013. Ice tectonic deformation during the rapid in situ drainage of a supraglacial lake on the Greenland Ice Sheet. *Cryosphere* 7:129–40

Durham WB, Heard HC, Kirby SH. 1983. Experimental deformation of polycrystalline H_2O ice at high pressure and low temperature: preliminary results. *J. Geophys. Res.* 88(S01):B377–92

Durham WB, Kirby SH, Stern LA. 1997. Creep of water ices at planetary conditions: a compilation. *J. Geophys. Res.* 102(E7):16293–302

Durham WB, Stern LA. 2001. Rheological properties of water ice—applications to satellites of the outer planets. *Annu. Rev. Earth Planet. Sci.* 29:295–330

Duval P, Ashby MF, Anderman I. 1983. Rate-controlling processes in the creep of polycrystalline ice. *J. Phys. Chem.* 87:4066–74

Eicken H, Grenfell TC, Perovich DK, Richter-Menge JA, Frey K. 2004. Hydraulic controls of summer Arctic pack ice albedo. *J. Geophys. Res.* 109(C8):C08007

Eicken H, Krouse HR, Kadko D, Perovich DK. 2002. Tracer studies of pathways and rates of meltwater transport through Arctic summer sea ice. *J. Geophys. Res.* 107(C10):8046

Flocco D, Feltham DL, Turner AK. 2010. Incorporation of a physically based melt pond scheme into the sea ice component of a climate model. *J. Geophys. Res.* 115(C8):C08012

Forster RR, Box JE, van den Broeke MR, Miege C, Burgess EW, et al. 2014. Extensive liquid meltwater storage in firn within the Greenland ice sheet. *Nat. Geosci.* 7:95–98

Fortt AL, Schulson EM. 2007. The resistance to sliding along Coulombic shear faults in ice. *Acta Mater.* 55:2253–64

Fortt AL, Schulson EM. 2011. Frictional sliding across Coulombic faults in first-year sea ice: a comparison with freshwater ice. *J. Geophys. Res.* 116(C11):C11012

Frankenstein G, Garner R. 1967. Equations for determining the brine volume of sea ice from −0.5° to −22.9°C. *J. Glaciol.* 6(48):349–58

Freitag J, Eicken H. 2003. Meltwater circulation and permeability of Arctic summer sea ice derived from hydrological field experiments. *J. Glaciol.* 49:349–58

Frey KE, Perovich DK, Light B. 2011. The spatial distribution of solar radiation under a melting Arctic sea ice cover. *Geophys. Res. Lett.* 38:L22501

Frost HJ, Ashby MF. 1982. *Deformation-Mechanism Maps*. Oxford, UK: Permagon

Gammon PH, Kiefte H, Clouter MJ, Denner WW. 1983. Elastic constants of artificial and natural ice samples by Brillouin spectroscopy. *J. Glaciol.* 29:433–60

Gharamti IE, Dempsey JP, Polojarvi A. 2021a. Creep and fracture of warm columnar freshwater ice. *Cryosphere* 15(5):2401–21

Gharamti IE, Dempsey JP, Polojärvi A, Tuhkuri J. 2021b. Fracture of warm S2 columnar freshwater ice: size and rate effects. *Acta Mater.* 202:22–34

Golden KM. 2001. Brine percolation and the transport properties of sea ice. *Ann. Glaciol.* 33:28–36

Golden KM, Ackley SF, Lytle VI. 1998. The percolation phase transition in sea ice. *Science* 282:2238–41

Golden KM, Eicken H, Heaton AL, Miner J, Pringle DJ, Zhu J. 2007. Thermal evolution of permeability and microstructure in sea ice. *Geophys. Res. Lett.* 34:L16501

Golding N, Durham WB, Prior DJ, Stern LA. 2020. Plastic faulting in ice. *J. Geophys. Res. Solid Earth* 125:e2019JB018749

Golding N, Renshaw CE, Burks CE, Lucas KN, Fortt AL, et al. 2013. Mechanical properties of the ice I–magnesium sulfate eutectic: a comparison with freshwater ice in reference to Europa. *Icarus* 225:248–56

Golding N, Schulson EM, Renshaw CE. 2010. Shear faulting and localized heating in ice: the influence of confinement. *Acta Mater.* 58:5043–56

Golding N, Schulson EM, Renshaw CE. 2012. Shear localization in ice: mechanical response and structural evolution during P-faulting. *Acta Mater.* 60:3616–31

Golding N, Snyder SA, Schulson EM, Renshaw CE. 2014. Plastic faulting in saltwater ice. *J. Glaciol.* 60:447–52

Griffith AA. 1925. The theory of rupture. In *Proceedings of the First International Congress of Applied Mechanics: Delft 1924*, ed. CB Biezeno, JM Burgers, pp. 55–63. Delft, Neth.: J. Waltman Jr.

Hammond NP, Barr AC, Cooper RF, Caswell TE, Hirth G. 2018. Experimental constraints on the fatigue of icy satellite lithospheres by tidal forces. *J. Geophys. Res. Planets* 123:390–404

Hansen CJ, Esposito L, Stewart AIF, Colwell J, Hendrix A, et al. 2006. Enceladus' water vapor plume. *Science* 311:1422–25

Hibler WD III, Schulson EM. 2000. On modeling the anisotropic failure and flow of flawed sea ice. *J. Geophys. Res.* 105(C7):17105–20

Hoppa G, Tufts BR, Greenberg R, Geissler P. 1999. Strike-slip faults on Europa: global shear patterns driven by tidal stress. *Icarus* 141(2):287–98

Horii H, Nemat-Nasser S. 1986. Brittle failure in compression: splitting, faulting and brittle-ductile transition. *Philos. Trans. R. Soc. A* 319:337–74

Howat IM, de la Pena S, van Angelen JH, Lenaerts JTM, van den Broeke MR. 2013. Expansion of meltwater lakes on the Greenland Ice Sheet. *Cryosphere* 7:201–4

Iliescu D, Murdza A, Schulson EM, Renshaw CE. 2017. Strengthening ice through cyclic loading. *J. Glaciol.* 63:663–69

Jaeger JC, Cook NGW. 1979. *Fundamentals of Rock Mechanics*. London: Chapman & Hall

Kawamura T, Ishikawa M, Takatsuka T, Kojima S, Shirasawa K. 2006. Measurements of permeability of sea ice. In *Proceedings of the 18th IAHR International Symposium on Ice, Sapporo, Japan, 28 August–1 September 2006*, ed. H Saeki, H Daigaku, pp. 105–12. Sapporo, Japan: Hokkaido Univ.

Kennedy FE, Schulson EM, Jones D. 2000. Friction of ice on ice at low sliding velocities. *Philos. Mag. A* 80:1093–110

Kietzig A-M, Hatzikiriakos SG, Englezos P. 2010. Physics of ice friction. *J. Appl. Phys.* 107:081101

Kilgore BD, Blanpied ML, Dieterich JH. 1993. Velocity dependent friction of granite over a wide range of conditions. *Geophys. Res. Lett.* 20:903–6

Kirchner HOK, Michot G, Schweizer J. 2000. Fracture toughness of snow in tension. *Philos. Mag. A* 80:1265–72

Krawczynski MJ, Behn MD, Das SB, Joughin I. 2009. Constraints on the lake volume required for hydro-fracture through ice sheets. *Geophys. Res. Lett.* 36:L10501

Kuehn GA, Schulson EM. 1994. The mechanical properties of saline ice under uniaxial compression. *Ann. Glaciol.* 19:39–48

Kwok R. 2001. Deformation of the Arctic Ocean sea ice cover: a qualitative survey. In *Scaling Laws in Ice Mechanics*, ed. JP Dempsey, HH Shen, pp. 315–22. New York: Springer

Lee RW, Schulson EM. 1988. The strength and ductility of ice under tension. *J. Offshore Mech. Arct. Eng.* 110:187–91

Lishman B, Sammonds P, Feltham D. 2011. A rate and state friction law for saline ice. *J. Geophys. Res.* 116(C5):C05011

Litwin KL, Zygielbaum BR, Polito PJ, Sklar LS, Collins GC. 2012. Influence of temperature, composition, and grain size on the tensile failure of water ice: implications for erosion on Titan. *J. Geophys. Res.* 117(E8):E08013

Ma RZ, Cao DY, Zhu CQ, Tian Y, Peng JB, et al. 2020. Atomic imaging of the edge structure and growth of a two-dimensional hexagonal ice. *Nature* 577:60–63

Makkonen L. 2012. A thermodynamic model of sliding friction. *AIP Adv.* 2:012179

Makkonen L, Tikanmäki M. 2014. Modeling the friction of ice. *Cold Reg. Sci. Technol.* 102:84–93

Marchenko A, Lishman B. 2017. The influence of closed brine pockets and permeable brine channels on the thermo-elastic properties of saline ice. *Philos. Trans. R. Soc. A* 375:20151351

Marko JR, Thomson RE. 1977. Rectilinear leads and internal motions in the ice pack of the western Arctic Ocean. *J. Geophys. Res.* 82(6):979–87

Marone C. 1998. The effect of loading rate on static friction and the rate of fault healing during the earthquake cycle. *Nature* 391:69–71

Marsan D, Stern H, Lindsay R, Weiss J. 2004. Scale dependence and localization of the deformation of Arctic sea ice. *Phys. Rev. Lett.* 93:178501

McCarthy C, Savage H, Nettles M. 2017. Temperature dependence of ice-on-rock friction at realistic glacier conditions. *Philos. Trans. R. Soc. A* 375:20150348

McClintock FA, Walsh JB. 1962. Friction of Griffith Cracks in Rock Under Pressure. *Proceedings of the 4th U.S. National Congress on Applied Mechanics*, ed. RM Rosenberg, MV Barton, RL Bisplinghoff, pp. 1015–22. New York: Am. Soc. Mech. Eng.

Miege C, Forster RR, Brucker L, Koenig LS, Solomon DK, et al. 2016. Spatial extent and temporal variability of Greenland firn aquifers detected by ground and airborne radars. *J. Geophys. Res. Earth Surf.* 121:2381–98

Miller O, Solomon DK, Miege C, Koenig L, Forster R, et al. 2020. Hydrology of a perennial firn aquifer in Southeast Greenland: an overview driven by field data. *Water Resour. Res.* 56:e2019WR026348

Molaro JL, Choukroun M, Phillips CB, Phelps ES, Hodyss R, et al. 2019. The microstructural evolution of water ice in the solar system through sintering. *J. Geophys. Res. Planets* 124:243–77

Montagnat M, Schulson EM. 2003. On friction and surface cracking during sliding. *J. Glaciol.* 49:391–96

Murdza A, Marchenko A, Schulson EM, Renshaw CE. 2021a. Cyclic strengthening of lake ice. *J. Glaciol.* 67:182–85

Murdza A, Polojärvi A, Schulson EM, Renshaw CE. 2021b. The flexural strength of bonded ice. *Cryosphere* 15:2957–67

Murdza A, Schulson EM, Renshaw CE. 2020. Strengthening of columnar-grained freshwater ice through cyclic flexural loading. *J. Glaciol.* 66:556–66

Murdza A, Schulson EM, Renshaw CE. 2021c. Behavior of saline ice under cyclic flexural loading. *Cryosphere* 15:2415–28

Murdza A, Schulson EM, Renshaw CE. 2022 Relaxation of flexure-induced strengthening of ice. *Geophys. Res. Lett.* 11:e2021GL096559

Nicolaus M, Katlein C, Maslanik J, Hendricks S. 2012. Changes in Arctic sea ice result in increasing light transmittance and absorption. *Geophys. Res. Lett.* 39:L24501

Nixon WA, Schulson EM. 1988. Fracture toughness of ice over a range of grain sizes. *J. Offshore Mech. Arct. Eng.* 110:192–96

Noda H, Shimamoto T. 2010. A rate- and state-dependent ductile flow law of polycrystalline halite under large shear strain and implications for transition to brittle deformation. *Geophys. Res. Lett.* 37:L09310

Olgin JG, Smith-Konter BR, Pappalardo RT. 2011. Limits of Enceladus's ice shell thickness from tidally driven tiger stripe shear failure. *Geophys. Res. Lett.* 38:L02201

Ono N, Kasai T. 1985. Surface-layer salinity of young sea ice. *Ann. Glaciol.* 6:298–99

Perovich DK, Grenfell TC, Light B, Hobbs PV. 2002. Seasonal evolution of the albedo of multiyear Arctic sea ice. *J. Geophys. Res.* 107(C10):8044

Persson BNJ. 2000. Friction dynamics for curved solid surfaces with long-range elasticity. *J. Chem. Phys.* 113:5477–84

Petrenko VF, Whitworth RW. 1999. *Physics of Ice*. Oxford, UK: Oxford Univ. Press

Polashenski C, Golden KM, Perovich DK, Skylingstad E, Arnsten A, et al. 2017. Percolation blockage: a process that enables melt pond formation on first year Arctic sea ice. *J. Geophys. Res. Oceans* 122:413–40

Polashenski C, Perovich D, Courville Z. 2012. The mechanisms of sea ice melt pond formation and evolution. *JJ. Geophys. Res.* 117(C1):C01001

Popovic P, Silber MC, Abbot DS. 2020. Critical percolation threshold restricts late-summer Arctic sea ice melt pond coverage. *J. Geophys. Res. Oceans* 125:e2019JC016029

Porco CC, Dones L, Mitchell C. 2017. Could it be snowing microbes on Enceladus? Assessing conditions in its plume and implications for future missions. *Astrobiology* 17(9):876–901

Postberg F, Schmidt J, Hillier J, Kempf S, Srama R. 2011. A salt-water reservoir as the source of a compositionally stratified plume on Enceladus. *Nature* 474:620–22

Pringle DJ, Miner JE, Eicken H, Golden KM. 2009. Pore space percolation in sea ice single crystals. *J. Geophys. Res.* 114(C12):C12017

Pritchard RS, Li G, Davis RO. 2012. A deterministic-statistical sea ice drift forecast model. *Cold Reg. Sci. Technol.* 76–77:52–62

Rampal P, Weiss J, Marsan D, Lindsay R, Stern H. 2008. Scaling properties of sea ice deformation from buoy dispersion analysis. *J. Geophys. Res.* 113(C3):C03002

Reinen LA, Tullis TE, Weeks JD. 1992. Two-mechanism model for frictional sliding of serpentinite. *Geophys. Res. Lett.* 19:1535–38

Renshaw CE. 1999. Connectivity of joint networks with power law length distributions. *Water Resour. Res.* 35:2661–70

Renshaw CE, Marchenko A, Schulson EM, Karulin E. 2018. Effect of compressive loading on first-year sea-ice permeability. *J. Glaciol.* 64:443–49
Renshaw CE, Schulson EM. 2001. Universal behavior in compressive failure of brittle materials. *Nature* 412:897–900
Renshaw CE, Schulson EM. 2017. Strength-limiting mechanisms in high-confinement, brittle-like failure: adiabatic transformational faulting. *J. Geophys. Res. Solid Earth* 122:1088–106
Renshaw CE, Schulson EM, Iliescu D. 2019. Experimental observation of the onset of percolation in fresh-water granular ice. *J. Geophys. Res. Solid Earth* 124:2445–56
Renshaw CE, Schulson EM, Iliescu D, Murdza A. 2020. Increased fractured rock permeability after percolation despite limited crack growth. *J. Geophys. Res. Solid Earth* 125:e2019JB019240
Richter-Menge JA, Jones KF. 1993. The tensile strength of first-year sea ice. *J. Glaciol.* 39:609–18
Richter-Menge JA, McNutt SL, Overland JE, Kwok R. 2002. Relating arctic pack ice stress and deformation under winter conditions. *J. Geophys. Res.* 107(C10):8040
Rist MA, Sammonds PR, Murrell SAF, Meredith PG, Doake CSM, et al. 1999. Experimental and theoretical fracture mechanics applied to Antarctic ice fracture and surface crevassing. *J. Geophys. Res.* 104(B2):2973–87
Saeki H, Ono T, Nakazawa N, Sakai M, Tanaka S. 1986. The coefficient of friction between sea ice and various materials used in offshore structures. *J. Energy Resour. Technol.* 108:65–71
Schreyer HL, Sulsky DL, Munday LB, Coon MD, Kwok R. 2006. Elastic-decohesive constitutive model for sea ice. *J. Geophys. Res.* 111(C11):C11S26
Schubnel A, Brunet F, Hilairet N, Gasc J, Wang Y, Green HW. 2013. Deep-focus earthquake analogs recorded at high pressure and temperature in the laboratory. *Science* 341:1377
Schulson EM. 1990. The brittle compressive fracture of ice. *Acta Metall. Mater.* 38:1963–76
Schulson EM. 2002. Compressive shear faults in ice: plastic vs. Coulombic faults. *Acta Mater*. 50:3415–24
Schulson EM. 2004. Compressive shear faults within arctic sea ice: fracture on scales large and small. *J. Geophys. Res.* 109(C7):C07016
Schulson EM. 2015. Low-speed friction and brittle compressive failure of ice: fundamental processes in ice mechanics. *Intern. Mater. Rev.* 60:451–78
Schulson EM. 2018. Friction of sea ice. *Philos. Trans. R. Soc. A* 376:20170336
Schulson EM, Duval P. 2009. *Creep and Fracture of Ice*. Cambridge, UK: Cambridge Univ. Press
Schulson EM, Fortt AL. 2012. Friction of ice on ice. *J. Geophys. Res.* 117(B12):B12204
Schulson EM, Fortt AL. 2013. Static strengthening of frictional surfaces of ice. *Acta Mater*. 61:1616–23
Schulson EM, Iliescu D, Renshaw CE. 1999. On the initiation of shear faults during brittle compressive failure: a new mechanism. *J. Geophys. Res.* 104(B1):695–705
Schulson EM, Kuehn GA. 1993. Ductile ice. *Philos. Mag. Lett.* 67:151–57
Schulson EM, Nodder ST, Renshaw CE. 2016. On the restoration of strength through stress-driven healing of faults in ice. *Acta Mater*. 117:306–10
Schweizer J, Michot G, Kirchner HOK. 2004. On the fracture toughness of snow. *Ann. Glaciol.* 38:1–8
Scourfield S, Sammonds P, Lishman B, Marchenko A. 2015. *The effect of sea ice rubble in ice-ice sliding*. Paper presented at 23rd International Conference on Port and Oceans Engineering under Arctic Conditions, Trondheim, Nor.
Serreze MC, Barrett AP, Stroeve JC, Kindig DN, Holland MM. 2009. The emergence of surface-based Arctic amplification. *Cryosphere* 3:11–19
Shimada M. 1992. Confirmation of two types of fracture in granite deformed at temperatures to 300°C. *Tectonophysics* 211:259–68
Smith-Konter B, Pappalardo RT. 2008. Tidally driven stress accumulation and shear failure of Enceladus's tiger stripes. *Icarus* 198:435–51
Snyder SA, Schulson EM, Renshaw CE. 2017. Effects of prestrain on the ductile-to-brittle transition of columnar ice. *Acta Mater*. 108:110–26
Stevens LA, Behn MD, McGuire JJ, Das SB, Joughin I, et al. 2015. Greenland supraglacial lake drainages triggered by hydrologically induced basal slip. *Nature* 522:73–76
Sukhorukov S, Loset S. 2013. Friction of sea ice on sea ice. *Cold Reg. Sci. Technol.* 94:1–12

Svetlizky I, Bayart E, Fineberg J. 2019. Brittle fracture theory describes the onset of frictional motion. *Annu. Rev. Condens. Matter Phys.* 10:253–73
Taylor D, Walsh M, Cullen A, O'Reilly P. 2016. The fracture toughness of eggshell. *Acta Biomater*. 37:21–27
Tsai VC, Stewart AL, Thompson AF. 2015. Marine ice-sheet profiles and stability under Coulomb basal conditions. *J. Glaciol.* 61:205–15
Tullis J, Yund RA. 1977. Experimental deformation of dry Westerly granite. *J. Geophys. Res.* 82(36):5705–18
van der Veen CJ. 2007. Fracture propagation as means of rapidly transferring surface meltwater to the base of glaciers. *Geophys. Res. Lett.* 34:L01501
Varshneya AK. 2006. *Fundamentals of Inorganic Glasses.* Boston: Academic
Wachter LM, Renshaw CE, Schulson EM. 2009. Transition in brittle failure mode in ice under low confinement. *Acta Mater*. 57:345–55
Wang Y, Hu X. 2017. Determination of tensile strength and fracture toughness of granite using notched three-point-bend samples. *Rock Mech. Rock Eng*. 50:17–28
Weeks WF, Ackley SF. 1986. The growth, structure and properties of sea ice. In *The Geophysics of Sea Ice*, ed. N Untersteiner, pp. 9–164. New York: Plenum
Weertman J. 1983. Creep deformation of ice. *Annu. Rev. Earth Planet. Sci.* 11:215–40
Weiss J, Dansereau V. 2017. Linking scales in sea ice mechanics. *Philos. Trans. R. Soc. A* 375:20150352
Weiss J, Schulson EM, Stern HL. 2007. Sea ice rheology in-situ, satellite and laboratory observations: fracture and friction. *Earth Planet. Sci. Lett.* 255:1–8
Wilchinsky AV, Feltham DL. 2011. Modeling Coulombic failure of sea ice with leads. *J. Geophys. Res.* 116(C8):C08040
Xu P, Cui B, Bu Y, Wang H, Guo X, et al. 2021. Elastic ice microfibers. *Science* 373(6551):187–92
Yasui M, Schulson EM, Renshaw CE. 2017. Experimental studies in mechanical properties and ductile-to-brittle transition of ice-silica mixtures: Young's modulus, compressive strength and fracture toughness. *J. Geophys. Res. Solid Earth* 122:6014–30
Yasutome A, Arakawa M, Maeno N. 1999. Measurements of ice-ice friction coefficients. *Seppyo* 61:437–43
Zwally HJ, Abdalati W, Herring T, Larson K, Saba J, Steffen K. 2002. Surface melt-induced acceleration of Greenland ice-sheet flow. *Science* 297:218–22

Annual Review
of Earth and
Planetary Sciences
Volume 50, 2022

Contents

Errata

An online log of corrections to *Annual Review of Earth and Planetary Sciences* articles may be found at http://www.annualreviews.org/errata/earth